



HAL
open science

**Environmentally Friendly
Lithium-Terephthalate/Polylactic Acid Composite
Filament Formulation for Lithium-Ion Battery
3D-Printing via Fused Deposition Modeling**

Alexis Maurel, Roberto Russo, Sylvie Grugeon, Stéphane Panier, Loic Dupont

► **To cite this version:**

Alexis Maurel, Roberto Russo, Sylvie Grugeon, Stéphane Panier, Loic Dupont. Environmentally Friendly Lithium-Terephthalate/Polylactic Acid Composite Filament Formulation for Lithium-Ion Battery 3D-Printing via Fused Deposition Modeling. *ECS Journal of Solid State Science and Technology*, 2021, 10 (3), 10.1149/2162-8777/abedd4 . hal-03608665

HAL Id: hal-03608665

<https://u-picardie.hal.science/hal-03608665>

Submitted on 6 Dec 2023

HAL is a multi-disciplinary open access archive for the deposit and dissemination of scientific research documents, whether they are published or not. The documents may come from teaching and research institutions in France or abroad, or from public or private research centers.

L'archive ouverte pluridisciplinaire **HAL**, est destinée au dépôt et à la diffusion de documents scientifiques de niveau recherche, publiés ou non, émanant des établissements d'enseignement et de recherche français ou étrangers, des laboratoires publics ou privés.

OPEN ACCESS

Environmentally Friendly Lithium-Terephthalate/Poly(lactic Acid) Composite Filament Formulation for Lithium-Ion Battery 3D-Printing via Fused Deposition Modeling

To cite this article: Alexis Maurel *et al* 2021 *ECS J. Solid State Sci. Technol.* **10** 037004

View the [article online](#) for updates and enhancements.

You may also like

- [Substituent Effects on Redox Potential of Organic Electrode Materials in Li/Na Rechargeable Batteries: Electronic Effects Vs. Cation-Substituents Interaction](#)
Sechan Lee, Jihyun Hong, Ji Eon Kwon *et al.*
- [Machine learning models to predict nitrate concentration in a river basin](#)
Diana Yáritza Dorado-Guerra, Gerald Corzo-Pérez, Javier Paredes-Arquiola *et al.*
- [Realization of the triple point of carbon dioxide in a transportable cell using long-stem SPRTs](#)
Yu Liang, J T Zhang, X J Feng *et al.*



245th ECS Meeting • May 26-30, 2024 • San Francisco, CA

Don't miss your chance to present!

Connect with the leading electrochemical and solid-state science network!

Deadline Extended: December 15, 2023

Submit now!





Environmentally Friendly Lithium-Terephthalate/Polylactic Acid Composite Filament Formulation for Lithium-Ion Battery 3D-Printing via Fused Deposition Modeling

Alexis Maurel,^{1,2,3,4,z}  Roberto Russo,^{1,3,5} Sylvie Grugeon,^{1,3}  Stéphane Panier,² and Loïc Dupont^{1,3,6,z}

¹Laboratoire de Réactivité et de Chimie des Solides, UMR CNRS 7314, Hub de l'Énergie, Université de Picardie Jules Verne, 80039 Amiens Cedex, France

²Laboratoire des Technologies Innovantes, LTI-EA 3899, Université de Picardie Jules Verne, 80025 Amiens, France

³RS2E, Réseau français sur le stockage électrochimique de l'énergie, FR CNRS 3459, 80039 Amiens Cedex, France

⁴The University of Texas at El Paso, El Paso, Texas 79968, United States of America

⁵Department Electric Equipment Laboratory (LME), EDF R&D, Avenue des Renardières, 77818 Morêt-sur-Loing Cedex, France

⁶Plateforme de Microscopie Électronique (PME) de l'Université de Picardie Jules Verne, Hub de l'Énergie, 80000 Amiens, France

In this paper, the development of an environmentally-friendly lithium-terephthalate/polylactic acid (Li₂TP/PLA) composite filament, for its use, once 3D-printed via Fused Deposition Modeling (FDM), as negative electrode of a lithium-ion battery is reported. Solvent-free formulation of the 3D-printable filament is achieved through the direct introduction of synthesized Li₂TP particles and PLA polymer powder within an extruder. Printability is improved through the incorporation of poly(ethylene glycol) dimethyl ether average $M_n \sim 500$ (PEGDME500) as plasticizer, while electrical performances are enhanced through the introduction of carbon black (CB). Thermal, electrical, morphological, electrochemical and printability characteristics are discussed thoroughly. By taking advantage of the 3D-printing slicer software capabilities, an innovative route is proposed to improve the liquid electrolyte impregnation within the 3D-printed electrodes.

© 2021 The Author(s). Published on behalf of The Electrochemical Society by IOP Publishing Limited. This is an open access article distributed under the terms of the Creative Commons Attribution 4.0 License (CC BY, <http://creativecommons.org/licenses/by/4.0/>), which permits unrestricted reuse of the work in any medium, provided the original work is properly cited. [DOI: 10.1149/2162-8777/abed44]



Manuscript submitted February 5, 2021; revised manuscript received February 23, 2021. Published March 19, 2021.

Paving the way towards the topological optimization of energy storage devices, their direct integration as well as the introduction of innovative design freedom,^{1,2} cutting-edge additive manufacturing (AM) techniques, also commonly called 3D-printing, have been recently employed to print lithium-ion batteries (LIB).^{3–5} Amongst the different available processes, thermoplastic material extrusion (TME), also commonly called fused deposition modeling (FDM), allows the elaboration of a complete LIB in one-single step without requiring any extra post-processes, unlike others 3D-printing techniques such as direct ink writing (DIW) or stereolithography apparatus (SLA) which generally require freeze drying, debinding and sintering. Employed as a material source for a classical FDM printer, thermoplastic filament is required. Introduced within the extruder head of the printer, the filament is then heated a few degrees above its melting temperature and selectively deposited through a computer-controlled nozzle.⁶ Layer after layer, the final 3D item is printed. Commercial FDM desktop 3D-printers exhibit a layer thickness resolution of about 150 μm for the first layer and down to 50 μm for the subsequent layers.

Since 2017, many studies have been focused on the formulation of composite 3D-printable filaments to print LIB components. So far, positive electrodes (PLA/LiFePO₄,^{7,8} PP/LiFePO₄,⁹ PLA/LMO¹⁰), negative electrodes (PLA/Graphite,^{7,11} PLA/LTO^{8,10}), but also separator (PLA/SiO₂⁷) and solid polymer electrolyte (PEO/LiTFSI,¹² PLA/PEO/LiTFSI¹³) have been reported. The formulation process always consists of a compromise between electrochemical and mechanical performances. Indeed, due to the FDM filament requirement, the loading of electrochemically active charges generally cannot exceed 30 vol% to maintain sufficient strength (conferred by the polymer matrix) to allow good printability. Nevertheless, as shown in our previous work,¹¹ this percentage can be further increased thanks to the introduction of an appropriate plasticizer, thus resulting in a final total amount of charges reaching up to 50 vol%. Thanks to the incorporation of a plasticizer additive such as poly(ethylene glycol) dimethyl ether

average $M_n \sim 500$ (PEGDME500) within the PLA matrix, our group was able for the first time to develop highly loaded PLA/graphite¹¹ and PLA/LiFePO₄⁷ filaments with up to 62 wt.% of active material respectively formulated as negative and positive electrodes. After optimization by introducing a conductive additive within the composite, negative electrode¹¹ (tested in a half-cell configuration using 1 M LiPF₆ in ethylene carbonate and diethyl carbonate as liquid electrolyte) depicted a reversible capacity of 200 mAh g⁻¹ of active material (99 mAh g⁻¹ of the total composite or also to 154.6 mAh cm⁻³) at current density of 18.6 mA g⁻¹ (C/20) after 6 cycles and 140 mAh g⁻¹ of active material (69 mAh g⁻¹ of the total composite or also 108.2 mAh cm⁻³) at current density of 37.3 mA g⁻¹ (C/10). Likewise, an optimized 3D-printed positive electrode developed by our group⁷ exhibited reversible capacity values of about 87 mAh g⁻¹ of active material (43 mAh g⁻¹ of the total composite or also to 77 mAh cm⁻³) at current density of 8.5 mA g⁻¹ (C/20), 45 mAh g⁻¹ of active material (22 mAh g⁻¹ of the total composite or also to 40 mAh cm⁻³) at a current density of 17 mA g⁻¹ (C/10), and 22 mAh g⁻¹ of active material (11 mAh g⁻¹ of the total composite or also to 20 mAh cm⁻³) at a current density of 34 mA g⁻¹ (C/5).

The introduction of corn-based PLA as a polymer matrix for 3D printing is an important step towards a green transition in battery manufacturing. This material, bio-sourced and easily recyclable, allows the construction of energy storage systems with a low environmental impact, as it greatly reduces environmental costs associated with the production of batteries currently available on the market. However, up to now the applications of 3D printing have always taken into consideration the “classic” inorganic electrochemically active materials present in the field of batteries, which are not free from problems related to finding resources and their location, as well as the costs of manufacturing and recyclability. Inorganic materials are based on transition metals such as cobalt, nickel and manganese, which are affected by supply and recyclability problems: (1) the abundance of such resources is strictly limited while the demand for energy storage systems seems endless; (2) their extraction and processing cost is very high; (3) LIB using inorganic materials are reported to be poorly recyclable. In the near

^zE-mail: alexis.maurel@u-picardie.fr; loic.dupont@u-picardie.fr

future, the high costs and ecological issues related to these materials could be the bottlenecks in the massive production of batteries, due to the enormous increase in demand for energy storage systems from the automotive and industrial fields.

Considering all these limitations, some groups have been already searching for innovative organic-based materials (made up of very abundant elements such as carbon, nitrogen, sulfur, oxygen and hydrogen) reported to be promising candidates for the production of batteries with an extremely low potential environmental footprint. Organic batteries are indeed particularly promising due to their easy material retrieval and recycling. The first study relating to organic molecules dates back to 1969, when Williams et al.¹⁴ presented a study on lithium-dichloroisocyanuric acid, a molecule where the reactivity is given by the carbonyl group, capable of storing energy through an electrochemical reaction involving lithium ions. However, this material has shown a number of problems, the most important of which is poor cycling, due to the rapid dissolution of the electrolyte in the solvent; most of the small organic molecules are in fact soluble in the classic organic solvents used for liquid electrolytes. Several other materials such as quinones, organodisulfides, nitroxyl radicals and imides,^{15–18} have been studied in an attempt to overcome the problems of poor cycling. Despite the efforts made by many research groups all over the world, most of the studied materials were shown to exhibit limited electrochemical performances upon cycling, thus leading in a gradual decrease in the attention towards the formulation of electrodes from organic molecules.

In 2008, following a work by Tarascon et al.¹⁹ on the lithium rhodizonate, the interest in organic materials was then revived, due to the relatively high performances depicted and the easy availability in nature. This compound, which belongs to the quinone class, has showed impressing electrochemical performance: capable of exchanging 4 lithium ions for a specific capacity of 580 mAh g⁻¹ with 87% of retention in the first cycle, an average potential of 2.8 V for an overall energy density of 1100 Wh kg⁻¹, this compound revealed outstanding performances, comparable with the inorganics materials on the market. The lithium salt can be obtained through a one-step acid-base reaction of Li base and rhodizonic acid: the latter has as a precursor a molecule called myo-inositol, a natural compound widely diffused in the plant world and present for about 8% of dry weight in corn-steeping liquor, a by-product of agricultural production. Lithium rhodizonate has become a milestone in the field of organic electrodes: the vast availability of green raw materials to produce it, together with the low cost and easy recyclability, has opened the way to the design of low-cost, bio-sourced organic materials for energy storage applications.

The same year, Armand and coworkers²⁰ published their work on lithium terephthalate (Li₂TP), a small molecule characterized by two carboxylic groups conjugated to an aromatic ring, capable of exchanging lithium ions at low potential, working as negative electrode. Similarly, this studied aroused great interest in the scientific community for the same reasons listed in the previous example: it is a green molecule, since its precursor, terephthalic acid, can be obtained as oxidative metabolism of p-xylene or through the simple degradation^{21,22} or biodegradation^{23,24} of a polyethylene terephthalate (PET), one of the most widespread polymer in the world, as it is widely used in the food sector, for the production of beverage containers (66%) and for food (8%),²⁵ and in the textile application.²⁶ Li₂TP combines, together with the ease and low cost of availability, also excellent electrochemical properties: the plateau is located at 0.8 V and is also capable of reversibly capturing 2.3 Li per unit formula, which translates into a specific capacity of approximately 300 mA h g⁻¹ at a rate of C/20. After 50 cycles, a residual capacity of 234 mAh.g⁻¹ was observed, reflecting the over cycling stability of this compound. In terms of rate capability, the Li₂TP showed a capacity of 240 mAh.g⁻¹ (70% of the theoretical capacity) at a rate of 1 C. This first study on lithium terephthalate have created a lot of interest in this small molecule, which was then studied both by modifying its structure^{27,28} and as a sodium²⁹ and

potassium salt.³⁰ Based on what has been reported in the literature, we decided to use Li₂TP as an active material for a 3D-printed electrode, both for its outstanding electrochemical performance and for its low environmental impact in terms of supply and recyclability.

In this context, herein for the first time, the development of an environmentally-friendly Li₂TP/PLA composite 3D-printable filament for its use, once 3D-printed via FDM, as a negative electrode of a LIB, is reported. As depicted hereafter, a solvent-free filament formulation protocol is established and an original route based on the 3D-printing slicer software capability is proposed to improve the liquid electrolyte impregnation and electrochemical performances of the 3D-printed electrodes. Samples thermal, electrical, morphological, electrochemical and printability characteristics are discussed thoroughly.

Experimental

Materials.—Polylactic acid powder was provided by NatureWorks, USA. Dichloromethane (DCM) solvent was supplied by VWR Chemicals, USA. Poly(ethylene glycol) dimethyl ether average M_n ~ 500 (PEGDME500), was purchased from Sigma Aldrich, Europe. Terephthalic acid (98% concentration) powder was provided by Alfa Aesar, Thermo Fisher Scientific, USA. LiOH·H₂O (98%) and KBr salt (99.5%) powders were purchased from Sigma Aldrich, Europe. Ethanol solvent was supplied by Sigma Aldrich, Europe. Carbon black Timcal Super (CB) (particle size: 20 nm, 45 m² g⁻¹), was supplied by Sigma Aldrich, USA. All solvents and reagents were used as received.

Synthesis of lithium terephthalate (Li₂TP).—Dilithium terephthalate was prepared via the procedure reported by Armand et al.³⁰ 60.0 g of terephthalic acid (0.361 mol) were transferred in a round flask and 250 ml of ethanol were added. 31.8 g of LiOH·H₂O (0.758 mol) were added to the reaction mixture, to provide a 10% of base excess; the reaction mixture was stirred overnight at room temperature. After the reaction time, the suspension was centrifuged and the precipitate was recovered. The product was washed three times with ethanol (3 × 100 ml) and dried overnight under vacuum at 150 °C. A white solid has been obtained with 91% of reaction yield.

Solvent-free composite filament formulation.—Afore-synthesized Li₂TP was combined with carbon black powder mixture (4:1 wt% ratio) and ball-milled for 15 min. The resulting powder was then combined with PLA powder and mixed using hand milling for 15 min. Finally, PEDGME500 plasticizer was added to obtain the final ratio PLA:Li₂TP:CB:PEGDME500 equals to 40:40:10:10 wt%. Resulting powder sample was manually mixed during 30 min. A Filabot Original extruder provided by Filabot Triex LLC, USA was directly fed consistently with the pre-mixed powder mixture to get standard 1.75 mm diameter 3D-printing filaments. No solvent was used in this protocol. Extruder temperature was set at 180 °C. The resulting filament was subsequently rolled around a spool by means of a Filabot spooler (Filabot Triex LLC, USA). The extruder was thoroughly purged with a neat PLA polymer matrix before extrusion of the sample. The resulting composite filament was stored in a controlled environment with low humidity and at low temperature to prevent the plasticizer evaporation.

Fused deposition modeling 3D-printing.—Electrodes cylinders (12.7 mm diameter, 200 μm or 600 μm thick) were designed with Autodesk Fusion 360 software after which they were sliced into 100 μm thick 2D-slices using PrusaSlicer software. Innovative porous (30% infill) rectilinear, gyroid and archimedean chords patterns (Fig. 7a) were generated. Electrodes were obtained with a Prusa MK3S 3D-printer (Prusa Research, Czech Republic). Thinner 3D-printed electrodes were employed to perform classical galvanostatic cycling while thicker ones (100% infill only) were used for

electrochemical impedance spectroscopy. Standard nozzle input and output diameters of 1.75 mm and 0.4 mm were used. As reported in our previous study,³¹ the highest resolution in the Z direction is 200 μm for the first layer and 50 μm for the following. The nozzle temperature was set 30 °C higher than the melting temperature of the filament obtained from differential scanning calorimetry. Bed temperature was set to 60 °C to favor the adherence of the first printed layer. Prior to printing, the nozzle was methodically purged by extruding a 2 cm^3 purge cube with the corresponding filament composition.

Thermal characterization.—Differential scanning calorimetry (DSC) of the filament and 3D-printed disc was carried out by means of a DSC204F1 supplied by NETZSCH-Gerätebau GmbH, Germany. Sample were characterized between –60 to 300 °C at a heating rate of 10 °C min^{-1} under argon atmosphere (50 mL min^{-1}), using about 10 mg of sample of each composition. Heat flow data from the first heating operation was recorded. Thermogravimetric analysis (TGA) of the synthesized Li_2TP powder was performed between 20 °C and 600 °C on a Netzsch thermal analyzer STA 449 C Jupiter equipped with a differential analysis microbalance coupled with a mass spectrometer QMS 403 Aeolos (heating rate: 5 C min^{-1} under argon flow).

Transmission infrared analysis (FTIR).—KBr pellets were made mixing Li_2TP and potassium bromide (spectroscopic grade) in a ratio 1:100. The resulting mixture was pressed using a 13 mm evacuable die set (Specac Ltd., UK) for IR pellet. The spectra were recorded, in transmission mode, using a Nicolet AVATAR 370 DTGS spectroscopy unit at room temperature, in a range of 4000 to 400 cm^{-1} with a resolution of 2 cm^{-1} .

Nuclear magnetic resonance (NMR).—BRUKER 400 MHz Avance III HD spectrometer was used to record synthesized- Li_2TP ^1H and ^{13}C NMR spectra (at 400 and 100 MHz, respectively) at 298 K. All the chemical shifts (δ) in this paper are reported in ppm relative to TMS. Deuterated dimethyl sulfoxide (d_6 -DMSO) and deuterium oxide (D_2O) were purchased from Sigma Aldrich (>99.5% purity).

Atomic absorption spectroscopy (AAS).— Li_2TP powder was characterized by AAS, using a AAnalyst 300 (Perkin-Elmer, USA), to determine the quantity of lithium in the salt. A lithium hollow-cathode lamp (wavelength: 670.8 nm) was used with a mixture oxidant/fuel of air:acetylene 5.8:1.

Electron microscopy.—The material dispersion and sample homogeneity were confirmed by means of a FEI Quanta200F (Thermo Fisher Scientific, USA) scanning electron microscope (SEM) in high vacuum mode. Secondary images were recorded with a 15 kV acceleration voltage. Filament and 3D-printed samples were cut in liquid nitrogen to obtain cross-sectional images.

Electrical conductivity characterization.—Electrochemical impedance spectroscopy experiments were performed with a MTZ-35 frequency response analyzer and an intermediate temperature system (ITS) supplied by BioLogic, France. The exact same procedure than the one reported in our previous work was followed.¹¹ Inductive phenomena from cables were first compensated by performing calibration of the empty ITS with the same cables. 3D-printed electrodes (600 μm thick) were subsequently introduced into a controlled environment sample holder (CESH). AC impedance measurement under air at temperatures varying from 20 °C to 90 °C (upon heating in steps of 10 °C) with an excitation voltage of 10 mV, a frequency range of 20 Hz to 0.05 Hz (20 points per decade and 10 measurements per point) and a soak time of 15 min were achieved. The resulting electronic conductivity and activation energy were deduced from the Nyquist and Phase-Bode plots of the complex impedance. Conductivities were calculated from the Eq. 1:

$$\sigma = \frac{1}{R} \times \frac{d}{A} \quad [1]$$

where d is the 3D-printed electrode thickness, A is the electrode surface area, and R is the respective resistances determined from the Nyquist and Bode plots.

Electrochemical characterization.—Swagelok-type cells were assembled in an Ar glovebox ($\text{H}_2\text{O} < 0.1$ ppm, $\text{O}_2 < 0.1$ ppm). Metallic lithium was used as a counter/reference electrode for half-cells while 3D-printed electrodes were employed as working electrodes. Fiberglass separator was provided by Whatman, GE Healthcare, USA. 150 μl of 1 M LiPF_6 in ethylene carbonate and diethyl carbonate (EC:DEC 1:1 weight ratio) supplied by Merck KGaA, Germany, was used as liquid electrolyte. Cells were galvanostatically discharged (lithiation) and charged (delithiation) at current densities of 8.16 mA g^{-1} (C/40), 16.33 mA g^{-1} (C/20) and 32.66 mA g^{-1} (C/10), between 0.05 and 2.0 V (vs Li/Li^+) by means of a BCS-805 (BioLogic, France) galvanostat. Serving here as reference, additional electrochemical tests were undergone on different powder mixtures and film. Powder mixture of Li_2TP :CB (wt% 80:20) and PLA: Li_2TP :CB:PEGDME500 (wt% 40:40:10:10) were thoroughly mixed in a mortar before testing. Composite film PLA: Li_2TP :CB:PEGDME500 (wt% 40:40:10:10) was obtained after drying of a tape-casted dichloromethane-based slurry. Electrochemical tests were performed at 20 °C.

Results and Discussions

Characterization of Li_2TP .—The synthesis of the electroactive material was performed by scaling up the synthesis previously reported in the literature by Armand et al.²⁰ The characterization of the reaction product was carried out using the classical methodologies, namely FTIR, NMR ^1H and ^{13}C (Fig. 1). The comparison of the Fourier transform infrared (FTIR) spectra of the starting reagent, terephthalic acid, and the corresponding dilithium salt shows significant differences: as depicted in Fig. 1a, the peak at 1671 cm^{-1} present in the terephthalic acid and which corresponds to the carboxylic acid (Fig. 1a, black line) is no longer present in the synthesized product, where instead there are two peaks relating to the asymmetric stretching and the symmetrical stretching of the $-\text{COOLi}$ group, respectively at 1569 cm^{-1} and 1390 cm^{-1} (Fig. 1a, red line). Finally, the complete disappearance of the wide band has been observed at 2600–3100 cm^{-1} , which refers to the vibration of the $-\text{OH}$ group, following the replacement of hydrogen with a lithium atom. The complete synthesis of the dilithium terephthalate salt was also confirmed by NMR analysis: the ^1H and ^{13}C spectra, respectively, are shown in Figs. 1b and 1c. In the ^1H spectra the disappearance of the peak at 13.28 ppm was witnessed, due to the presence of the hydrogen of the $-\text{OH}$ group of the terephthalic acid (Fig. 1b, black line), in addition to the shift of the signal related to the hydrogens of the aromatic ring, which is shifted from 8.05 ppm to 7.81 ppm following the lithiation of the carboxy groups. Furthermore, in the spectrum of Li_2TP there are no other peaks except that related to the solvent used for the analysis, as confirmation of the absence of traces of impurities or of the reaction solvent. Finally, comparing the ^{13}C spectra, the most significant difference is that relating to the peak of the carbon C=OO: in the case of the starting acid, the signal relating to this carbon is found at 167.13 ppm (Fig. 1c, black line), while for the lithium salt the peak is shifted to 175.31 ppm, due to the presence of the metal ion. The complete chemical formula of the compound was $\text{Li}_{2.03\pm 0.05}\text{-TP}$ as deduced by AAS for the Li content. The thermogravimetric measurement (TG) was employed to investigate the solvation degree: the analysis (Fig. 1d) showed a weight loss of about 0.11% up to 400 °C and a loss of 0.48% up to ca. 500 °C. Therefore, we can deduce that the synthesized molecule is not in a solvated state, as no weight loss was found after heating up to 500 °C.

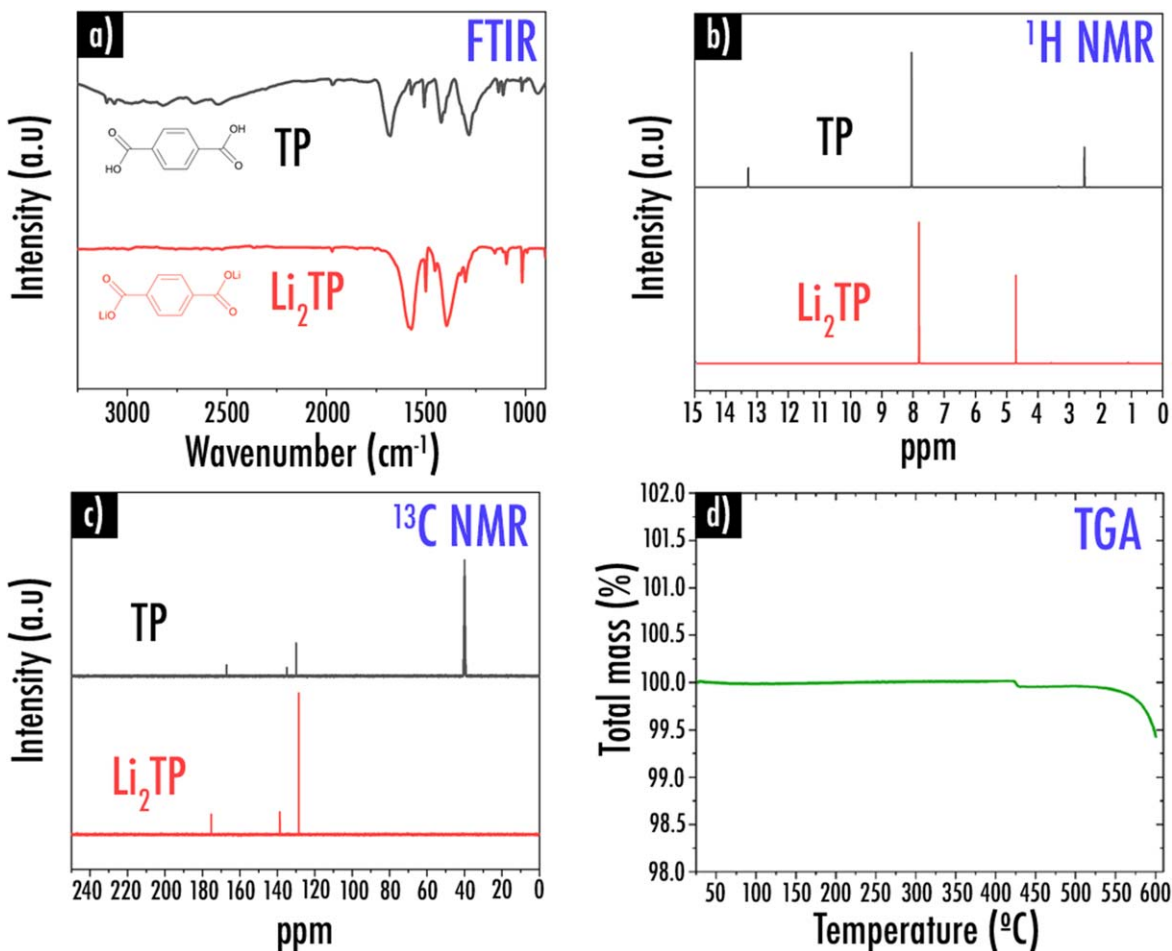


Figure 1. Characterization of Li₂TP. Comparison of Li₂TP (red lines) and TP (black line) spectra of a) FTIR, b) ¹H NMR, c) ¹³C NMR. In the box d) is reported the TGA analysis.

Solvent free 3D-printable filament formulation.—Based on our previous research,^{7,9,11,12,32} the formulation of a composite filament, here comprising PLA:Li₂TP:CB:PEGDME500 (wt% 40:40:10:10), and specially designed to be used as a negative electrode within a LIB, was initiated. While one of the classical elaboration protocols usually involves the development of composite films by tape-casting, requiring the use of an important quantity of solvents (DCM to dissolve PLA pellets and ensure good homogeneity¹¹), it was here decided to develop a more environmental-friendly protocol. Thus, solvent-demanding tape-casting step was removed and rather replaced by a series of solvent-free mechanical mixing steps (ball and hand-milling) of the different powder mixture (cf Experimental part). Figure 2 displays the complete elaboration process.

In this work, a single screw extruder was used, however it is important to mention that at least 80 g of composite materials was required to obtain subsequently a homogeneous filament sample corresponding to the desired composition. A double screw extruder may be employed in the future as it could ensure great filament homogeneity while introducing only a few grams of material into the hopper. Here, after extrusion, the inner composite filament homogeneity was confirmed by performing SEM experiments. As displayed in Fig. 3a, previously synthesized pure Li₂TP particles are between 1 and 10 μm. These latter appear to be particularly well distributed within the PLA polymer matrix of the composite filament (Fig. 3b).

Electrodes 3D-printing via desktop fused deposition modeling.—Before performing 3D-printing, the afore-prepared composite filament containing PLA, Li₂TP, CB and PEGDME500, was

characterized via DSC. From this experiment, as depicted in Fig. 4, PEGDME500 melting temperature appeared at about 5 °C, the crystallization temperature at 75 °C, while the melting temperature (T_m) of the composite filament emerged at 142 °C. From these values, it was subsequently decided to set the nozzle temperature at 172 °C, or 30 °C higher than the melting temperature of the filament, to perform 3D-printing of the electrode discs. From Eq. 2, the percentage of crystallinity of the polymer matrix within the filament and 3D-printed electrode (100% infill) was determined:

$$X_c = \frac{\Delta H_m - \Delta H_c}{w \cdot \Delta H_{100}} \cdot 100 \quad [2]$$

where ΔH_m is the value of melting enthalpy, ΔH_c is the crystallization enthalpy, ΔH_{100} is the enthalpy of the completely crystalline PLA serving here as reference (93.6 J/g for PLA^{15,33}), and w is the weight fraction of polymer in the sample. While from the DSC experiments, it was demonstrated that neat PLA depicts a crystallinity of 42%, here, a crystallinity of about 8% (not considering the plasticizer evaporation) was calculated from the composite PLA/Li₂TP/CB/PEGDME500 filament and down to 7% for the 3D-printed disc. This latter value is in good agreement with what was observed previously in literature: according to Ragones et al.,¹³ such behavior may be explained by the formation, at high temperature under constraint, of a PLA mesophase, between amorphous and crystalline, that is prone to melt quickly upon printing, thus resulting in chain randomization and release of the constraints on the thermodynamic relaxation of the oriented amorphous chains.

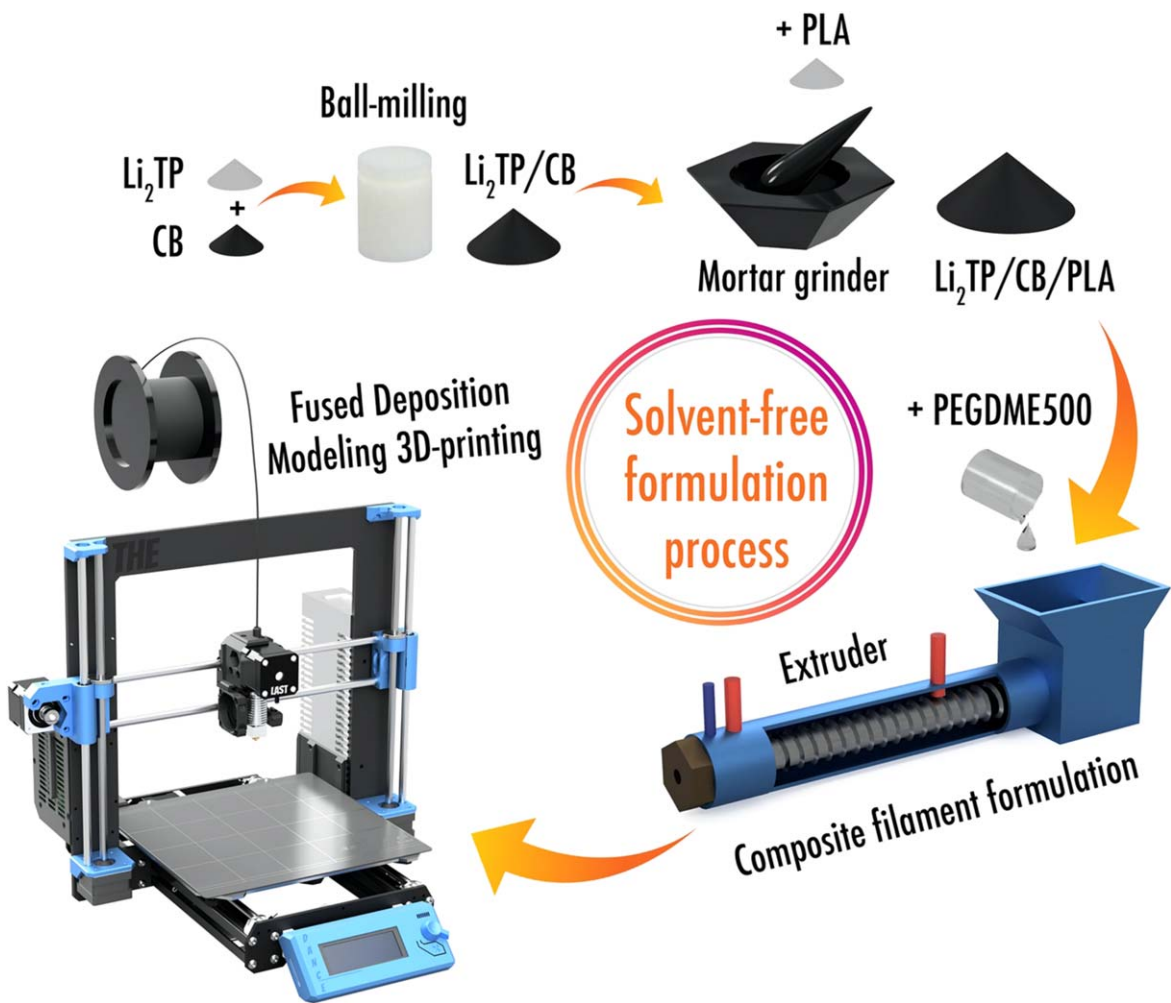


Figure 2. Solvent-free elaboration process.

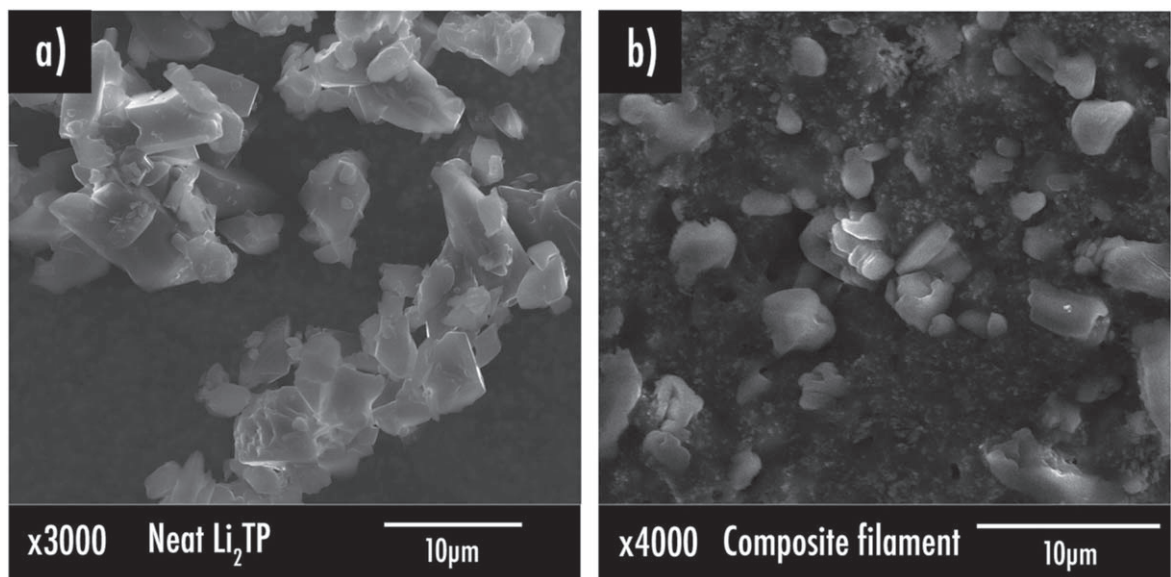


Figure 3. Secondary Electron SEM images depicting the (a) neat Li_2TP particles; (b) the composite filament produced $\text{PLA}:\text{Li}_2\text{TP}:\text{CB}:\text{PEGDME500}$ (wt% 40:40:10:10).

Figure 5 exhibits the EIS results of the $\text{PLA}:\text{Li}_2\text{TP}:\text{CB}:\text{PEGDME500}$ (wt% 40:40:10:10) 3D-printed disc sample. Transversal section was here characterized. While an important amount of CB was added to the

electrode, it is important to mention that conductivity of the resulting 3D-printed electrode disc is still limited ($1 \times 10^{-9\text{S}} \cdot \text{cm}^{-1}$ at 20°C and up to $2 \times 10^{-8\text{S}} \cdot \text{cm}^{-1}$ at 90°C) in comparison with previously reported

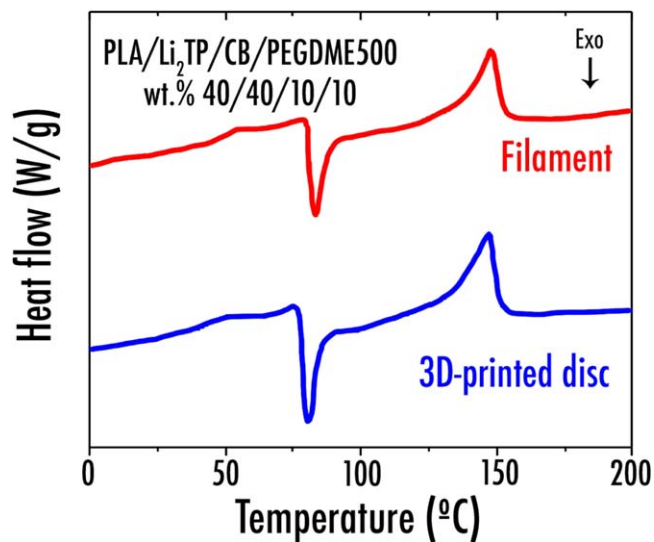


Figure 4. DSC curve for the composite filament and 3D-printed disc (PLA:Li₂TP:CB:PEGDME500 wt% 40:40:10:10).

PLA/LiFePO₄ ($7 \times 10^{-25} \cdot \text{cm}^{-1}$ at 20 °C⁷) or PLA/graphite ($0.4 \text{S} \cdot \text{cm}^{-1}$ at 20 °C¹¹) electrodes. This behavior can be explained by the very poor conductivity conferred by organic materials such as Li₂TP. As confirmed later in this article (electrochemical characterization), this poor electronic conductivity is expected to lead to poor electrochemical performances. Finally, it is worth mentioning that tests had been performed to further increase the CB amount with a view to finally enhance the electrical conductivity of the electrode. Unfortunately, such composite filament containing an amount of CB higher than 40 wt.% was too brittle and not printable. To determine the best compromise between the electrical performances and printability, future studies may be dedicated on the development of 3D-printing filament via co-extrusion. Therefore, charges (Li₂TP and CB) could be concentrated in the central part of the filament while a thin coating of pure polymer matrix would wrap it. Such co-extruded filament would undoubtedly be much easier to print as it would considerably prevent nozzle from clogging issues. Composite filaments with a higher amount of charges and thus more electronically conductive and electrochemically promising could be developed.

Comparison of electrochemical properties of different formulation.—In order to better understand the influence of composite formulation on the electrochemical performances, two galvanostatic tests were carried out on two different powders with different ratios of active material. As already mentioned in the previous paragraphs, the optimal formulation, in order to conjugate both the mechanical and electrochemical properties, was found to be PLA/Li₂TP/CB/PEGDME500 with a wt.% ratio 40/40/10/10. The ratio between active material and conductive carbon was here 4:1, higher than the ratio reported in the literature, equivalent to 2.33:1.²⁰ As a result, this can strongly influence the electrochemistry of the electrode, in particular the specific capacity. This difference in conductive carbon content could affect the electrical percolation, since organic materials are electric insulators and they require a large quantity of conductive carbon. Galvanostatic tests were performed using Swagelok-type half-cell vs lithium disc, in a potential window of 2.0–0.05 V at different C-rate (C/40, C/20 and C/10). The powder of Li₂TP/CB 4:1 was the first formulation that has been investigated; the galvanostatic profiles obtained at different current density are reported in Fig. 6a. During the first cycle, the discharge capacity was 237 mAh g⁻¹, while the reversible capacity (charging phase) was 118 mAh g⁻¹: this result deeply differs from the capacity observed in previous works (300 mAh g⁻¹), where the mass ratio between active material and carbon was 2.33:1. Moreover, also the rate performance turns out to be rather low, as the reversible capacity drops to

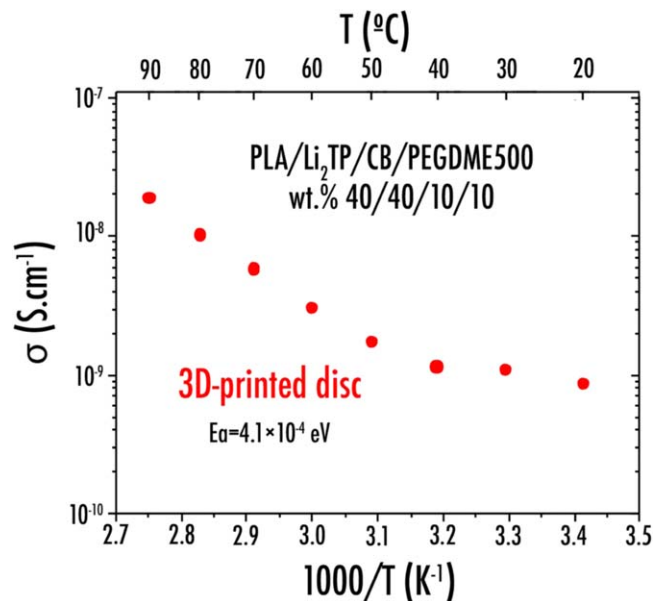


Figure 5. Arrhenius plot of the electrical conductivity for PLA:Li₂TP:CB:PEGDME500 (wt% 40:40:10:10) 3D-printed disc sample.

73 and 47 mAh g⁻¹ at C-rate of C/20 and C/10, respectively. In addition, the performance of PLA/Li₂TP/CB composite (4:4:1 wt.% ratio) was analyzed, in order to evaluate the influence of the polymeric matrix on the electrochemical properties (Fig. 6b). In the first discharge plateau, a capacity of 424 mAh g⁻¹ was observed, approximately double of what was measured in the previous case: this phenomenon can be explained by a different SEI layer formation, which leads to a higher amount of irreversible capacity during the first cycle. However, the reversible capacity remained very high, around 88 mAh g⁻¹, not far from that observed for Li₂TP/CB formulation. At higher C-rate, the capacity decreases to 24 mAh g⁻¹ at C/20 and 11 mAh g⁻¹ at C/10.

Li₂TP-based electrode 3D-printed discs.—The aforementioned Li₂TP-based filament was subsequently introduced as a material source to feed the FDM 3D-printer. Resulting 3D-printed electrode discs (200 μm) with different infill 30% patterns (archimedean chords, gyroid and rectilinear) were finally obtained (Fig. 7) and their corresponding electrochemical performance as negative electrode was investigated (Fig. 6c). The 3D-printed Li₂TP/PLA/C45/PEGDME500 discs were galvanostatically cycled in a Swagelok-type half-cell versus lithium metal. The first step was to print a disc with a geometry called rectilinear. This electrode showed poor electrochemistry: the first discharge at C/40 was quantified to only 0.8 mAh g⁻¹, with a reversible capacity on the first cycle of 0.54 mAh g⁻¹. This very low capacity can be explained by the 3D architecture of the electrode: the high infill density hinders the electrolyte impregnation along the entire thickness of the electrode. Consequently, the electrolyte remains only on the surface and cannot reach the entire volume of the disc, not allowing all the active material present in the electrode to react electrochemically. Even in the following cycles the capacity remains about 0.5 mAh g⁻¹ at C/40, and then decreases to 0.36 mAh g⁻¹ at the C-rate of C/20 and 0.21 mAh g⁻¹ at C/10. This test on the first 3D printed electrode highlights a problem with the diffusion of the electrolyte over the entire electrode: in order to investigate this phenomenon, two other discs with different geometry have been built. For the first, a gyroid-type geometry was used, with an infill of 30% as a print parameter. This geometry allows a better distribution of the electrolyte inside the electrode, thus allowing it to obtain a greater capacity. In the first cycle, a discharge capacity of 3.67 mAh g⁻¹ was observed, with a reversible capacity of 1.8 mAh g⁻¹ at C/40. At higher C-rate, it shows a reversible capacity of 1 mAh g⁻¹ and 0.45 mAh g⁻¹ at C/20 at C/10 C-rate, respectively.

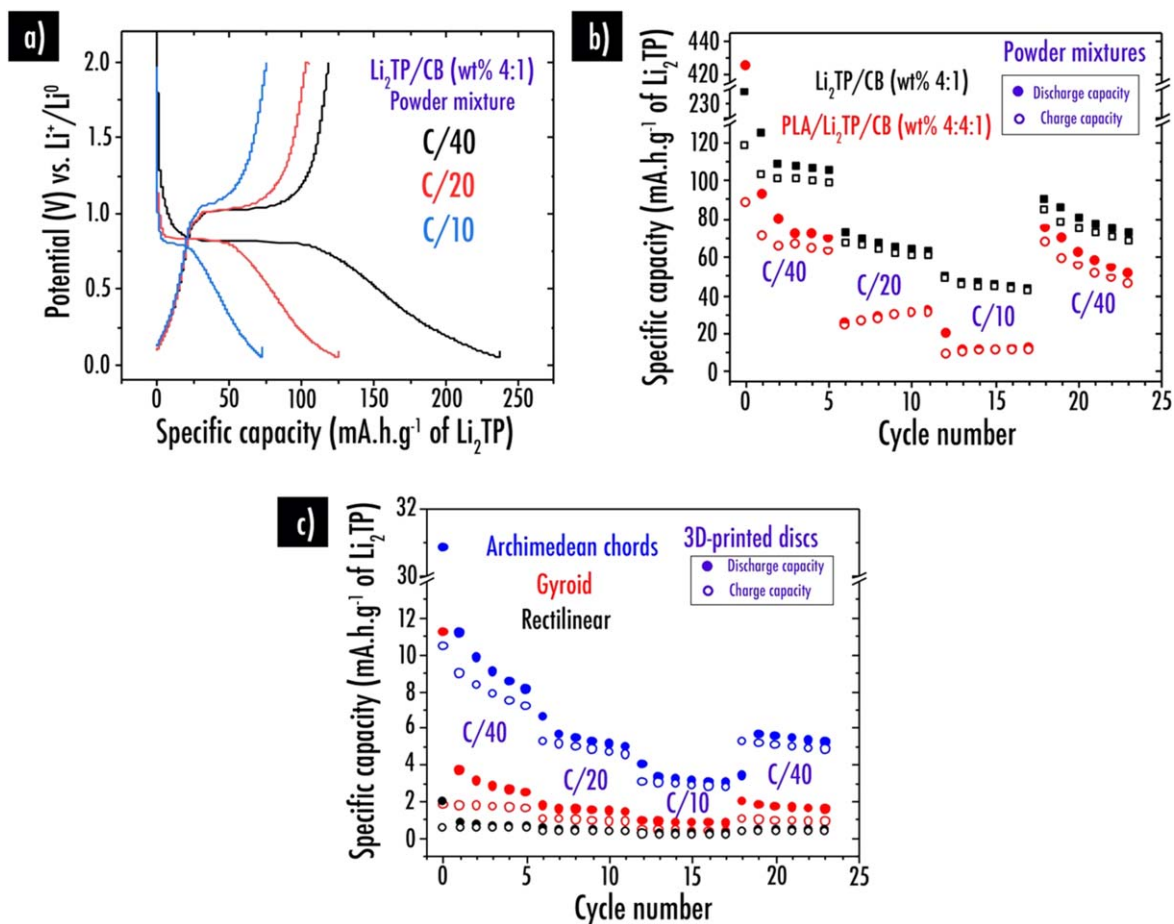


Figure 6. (a) Charge/discharge capacity profiles for the $\text{Li}_2\text{TP}/\text{CB}$ (wt.% 4:1) powder mix sample; (b) Capacity retention plots at different C-rate for $\text{Li}_2\text{TP}/\text{CB}$ (wt.% 4:1) and $\text{PLA}/\text{Li}_2\text{TP}/\text{CB}$ (wt.% 4:4:1) powder mixture; (c) Capacity retention plots at different C-rate for $\text{PLA}/\text{Li}_2\text{TP}/\text{CB}/\text{PEGDME500}$ (wt.% 40:40:10:10) 3D-printed discs with various infill patterns (archimedean chords, gyroid and rectilinear).

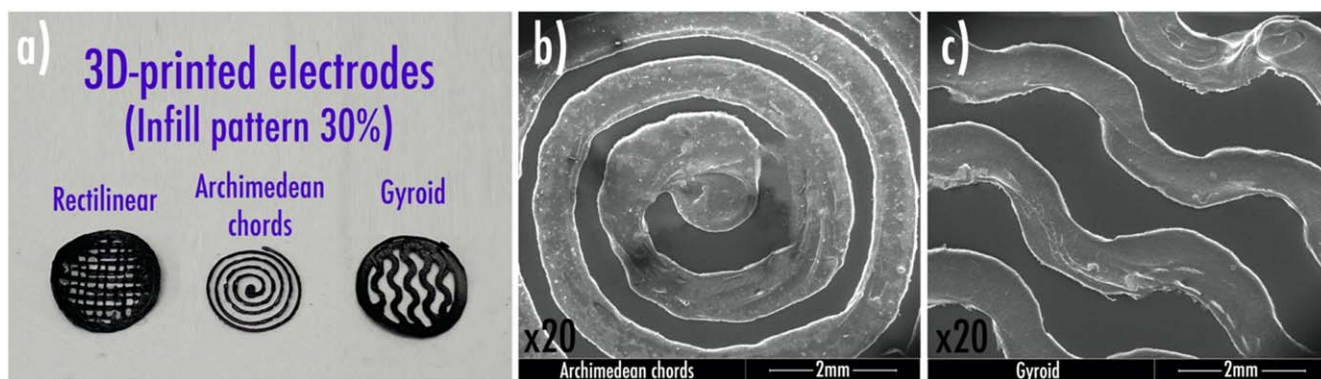


Figure 7. (a) 3D-printed $\text{PLA}:\text{Li}_2\text{TP}:\text{CB}:\text{PEGDME500}$ (wt% 40:40:10:10) electrodes with various infill patterns; Secondary electron SEM images of the 3D-printed electrodes based on a (b) archimedean chords infill pattern; (c) gyroid infill pattern.

When passing from rectilinear to gyroid geometry, it confirmed the importance of electrode's shape, despite the observed specific capacity was still far from that of the simple composite $\text{Li}_2\text{TP}/\text{C45}$ powder. It has directed our efforts towards improving the electrode geometry, as this is a key parameter in order to improve the impregnation of the active material and consequently its electrochemical performance. The last electrode was printed with an archimedean chords pattern, which consists in a spiral shape characterized by the equidistance of all the loops that compose it.

The first discharge showed $31 \text{ mA}\cdot\text{h}\cdot\text{g}^{-1}$, three times higher compared to gyroid electrode, with $10 \text{ mA}\cdot\text{h}\cdot\text{g}^{-1}$ of reversible capacity at C/40. At higher C-rate, this electrode showed $5.3 \text{ mA}\cdot\text{h}\cdot\text{g}^{-1}$ of specific capacity at C/20 and $3 \text{ mA}\cdot\text{h}\cdot\text{g}^{-1}$ at C/10. Electrochemical performances could be further improved in the future by performing machine modifications: a smaller outlet diameter of the nozzle (0.2 mm or 0.1 mm) could be employed to improve the resolution and obtain thinner electrodes. However, it may raise printing issues such as nozzle clogging (charges particles

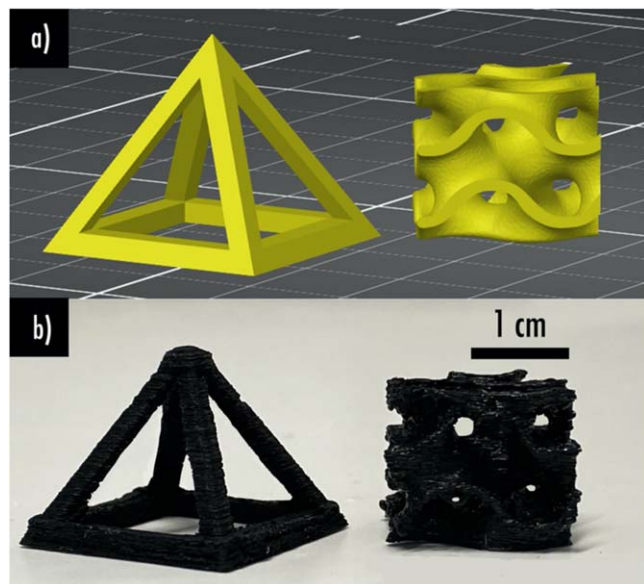


Figure 8. (a) Designed and (b) 3D-printed of PLA:Li₂TP:CB:PEGDME500 (wt% 40:40:10:10) three-dimensional complex electrode architectures.

being stuck in the nozzle resulting in extrusion issues). Finally, while such printed electrodes are still planar so far, the printability of complex three-dimensional architectures (pyramid and gyroid objects) was also demonstrated as depicted in Fig. 8. In the future, using a FDM 3D-multimaterial printing option,³⁴ the printability in one single step of a complete battery could be envisioned. This paves the way towards the topological optimization of the energy storage within the final object with a view to maximize the electrochemical performances while reducing considerably the dead-volume.

Conclusion

This work was focused on the development of an environmentally-friendly lithium-terephthalate/poly(lactic acid) (Li₂TP/PLA) composite filament, for its use, once 3D-printed via Fused Deposition Modeling (FDM), as negative electrode of a lithium-ion battery. A solvent-free formulation protocol to develop a composite electrode 3D-printable filament was established. The 3D-printable filament was here obtained through the introduction of synthesized Li₂TP and PLA polymer powders within an extruder. Printability is improved through the incorporation of poly(ethylene glycol) dimethyl ether average $M_n \sim 500$ (PEGDME500) as plasticizer, while electrical performances are enhanced through the introduction of carbon black (CB). While electrochemical performances of the printed electrodes are relatively low due the poor electronic conductivity and poor liquid electrolyte impregnation, an innovative route involving the use of the slicer software to propose custom-shaped electrodes (infill pattern) to improve the liquid electrolyte impregnation within the 3D-printed electrodes was demonstrated. This preliminary study paves the way towards the next generation of 3D-printed lithium ion batteries by FDM.

Acknowledgments

This work was supported by the Fonds Européen de Développement Régional (FEDER), the Conseil Régional des Hauts-de-France and the Université de Picardie Jules Verne (UPJV). The authors would like to thank M. Courty for technical assistance (DSC), Michel Armand for discussions, and the UPJV microscopy platform for sharing their facilities.

ORCID

Alexis Maurel  <https://orcid.org/0000-0001-8245-9621>
Sylvie Grugeon  <https://orcid.org/0000-0002-3119-6806>

References

1. L. F. Arenas, F. C. Walsh, and C. P. de Leon, "3D-printing of redox flow batteries for energy storage: a rapid prototype laboratory cell." *ECS J. Solid State Sci. Technol.*, **4**, P3080 (2015).
2. H. Sun et al., "Vanadium redox flow batteries fabricated by 3D printing and employing recycled vanadium collected from ammonia slag." *J. Electrochem. Soc.*, **166**, B3125 (2019).
3. V. Egorov, U. Gulzar, Y. Zhang, S. Breen, and C. O'Dwyer, "Evolution of 3D printing methods and materials for electrochemical energy storage." *Adv. Mater.*, **32** (2020).
4. U. Gulzar, C. Glynn, and C. O'Dwyer, "Additive manufacturing for energy storage: methods, designs and material selection for customizable 3D printed batteries and supercapacitors." *Current Opinion in Electrochemistry*, **20**, 46 (2020).
5. M. P. Browne, E. Redondo, and M. Pumerá, "3D printing for electrochemical energy applications." *Chem. Rev.*, **120**, 2783 (2020).
6. D. M. Stevens, B. L. Gray, D. B. Leznoff, H. Furukawa, and A. Khosla, "3D printable vapochromic sensing materials." *J. Electrochem. Soc.*, **167**167503 (2020).
7. A. Maurel, S. Grugeon, B. Fleutot, M. Courty, K. Prashantha, H. Tortajada, M. Armand, S. Panier, and L. Dupont, "Three-dimensional printing of a LiFePO₄/graphite battery cell via fused deposition modeling." *Sci. Rep.*, **9**, 18031 (2019).
8. H. Ragonés, S. Menkin, Y. Kamir, A. Gladkikh, T. Mukra, G. Kosa, and D. Golodnitsky, "Towards smart free form-factor 3D printable batteries." *Sustainable Energy & Fuels*, **2**, 1542 (2018).
9. A. Maurel and M. Haukka et al., "Considering lithium-ion battery 3D-printing via thermoplastic material extrusion and polymer powder bed fusion." *Additive Manufacturing*, **37**, 101651 (2021).
10. C. Reyes, R. Somogyi, S. Niu, M. A. Cruz, F. Yang, M. J. Catenacci, C. P. Rhodes, and B. J. Wiley, "Three-dimensional printing of a complete lithium ion battery with fused filament fabrication." *ACS Appl. Energy Mater.*, **1**, 5268 (2018).
11. A. Maurel, M. Courty, B. Fleutot, H. Tortajada, K. Prashantha, M. Armand, S. Grugeon, S. Panier, and L. Dupont, "Highly loaded graphite-poly(lactic acid) composite-based filaments for lithium-ion battery three-dimensional printing." *Chem. Mater.*, **30**, 7484 (2018).
12. A. Maurel, M. Armand, S. Grugeon, B. Fleutot, C. Davoisne, H. Tortajada, M. Courty, S. Panier, and L. Dupont, "Poly(Ethylene Oxide)-LITFSI solid polymer electrolyte filaments for fused deposition modeling three-dimensional printing." *J. Electrochem. Soc.*, **167** (2020).
13. H. Ragonés, A. Vinegrad, G. Ardel, M. Goor, Y. Kamir, M. M. Dorfman, A. Gladkikh, and D. Golodnitsky, "On the road to a multi-coaxial-cable battery: development of a novel 3d-printed composite solid electrolyte." *J. Electrochem. Soc.*, **167**, 070503 (2019).
14. D. L. Williams, J. J. Byrne, J. S. Driscoll, and A. High, "Energy density lithium/dichloroisocyanuric acid battery system." *J. Electrochem. Soc.*, **116**, 2 (1969), &.
15. Z. P. Song and H. S. Zhou, "Towards sustainable and versatile energy storage devices: an overview of organic electrode materials." *Energy Environ. Sci.*, **6**, 2280 (2013).
16. A. Mauger, C. Julien, A. Paoletta, M. Armand, and K. Zaghib, "Recent progress on organic electrodes materials for rechargeable batteries and supercapacitors." *Materials*, **12**, 11 (2019).
17. M. E. Bhosale, S. Chae, J. M. Kim, and J. Y. Choi, "Organic small molecules and polymers as an electrode material for rechargeable lithium ion batteries." *J. Mater. Chem. A*, **6**, 19885 (2018).
18. P. Poizot, J. Gaubicher, S. Renault, L. Dubois, Y. Liang, and Y. Yao, "Opportunities and challenges for organic electrodes in electrochemical energy storage." *Chem. Rev.*, **120**, 6490 (2020).
19. J. M. Tarascon, "Towards sustainable and renewable systems for electrochemical energy storage." *ChemSusChem*, **1**, 777 (2008).
20. M. Armand, S. Grugeon, H. Vezin, S. Laruelle, P. Ribiere, P. Poizot, and J. M. Tarascon, "Conjugated dicarboxylate anodes for Li-ion batteries." *Nat. Mater.*, **8**, 120 (2009).
21. V. A. Kosmidis, D. S. Achilias, and G. P. Karayannidis, "Poly(ethylene terephthalate) recycling and recovery of pure terephthalic acid. Kinetics of a phase transfer catalyzed alkaline hydrolysis." *Macromol. Mater. Eng.*, **286**, 640 (2001).
22. T. Masuda, Y. Miwa, A. Tamagawa, S. R. Mukai, K. Hashimoto, and Y. Ikeda, "Degradation of waste poly(ethylene terephthalate) in a steam atmosphere to recover terephthalic acid and to minimize carbonaceous residue." *Polym. Degrad. Stab.*, **58**, 315 (1997).
23. J. F. Zhang, X. C. Wang, J. X. Gong, and Z. Y. Gu, "A study on the biodegradability of polyethylene terephthalate fiber and diethylene glycol terephthalate." *J. Appl. Polym. Sci.*, **93**, 1089 (2004).
24. R. Koshti, L. Mehta, and N. Samarth, "Biological recycling of polyethylene terephthalate: a mini-review." *J. Polym. Environ.*, **26**, 3520 (2018).
25. B. Kuczynski and R. Geyer, "Material flow analysis of polyethylene terephthalate in the US, 1996-2007." *Resour. Conserv. Recycl.*, **54**, 1161 (2010).
26. E. M. Aizenshtein, "Polyester fibres continue to dominate on the world textile raw materials balance sheet." *Fibre Chem.*, **41**, 1 (2009).

27. A. E. Lakraychi, F. Dolhem, F. Djedaini-Pilard, A. Thiam, C. Frayret, and M. Becuwe, "Decreasing redox voltage of terephthalate-based electrode material for Li-ion battery using substituent effect." *J. Power Sources*, **359**, 198 (2017).
28. A. E. Lakraychi, F. Dolhem, F. Djedaini-Pilard, and M. Becuwe, "Substituent effect on redox potential of terephthalate-based electrode materials for lithium batteries." *Electrochem. Commun.*, **93**, 71 (2018).
29. Y. Park, D. S. Shin, S. H. Woo, N. S. Choi, K. H. Shin, S. M. Oh, K. T. Lee, and S. Y. Hong, "Sodium terephthalate as an organic anode material for sodium ion batteries." *Adv. Mater.*, **24**, 3562 (2012).
30. Q. J. Deng, C. C. Tian, and Z. B. Luo, "Atomic layer deposition of Al₂O₃ on organic potassium terephthalate with enhanced K-storage behavior for K-ion batteries." *Ionic*s, **26**, 1805 (2020).
31. A. Maurel, S. Grugeon, M. Armand, B. Fleutot, M. Courty, K. Prashantha, C. Davoisne, H. Tortajada, S. Panier, and L. Dupont, "Overview on lithium-ion battery 3D-Printing By means of material extrusion." *ECS Trans.*, **98**, 3 (2020).
32. A. Maurel, *PhD Thesis - Thermoplastic Composite Filaments Formulation and 3D-Printing of a Lithium-Ion Battery Via Fused Deposition Modeling*, Université de Picardie Jules Verne (Amiens, France) (2020).
33. F. J. Li, S. D. Zhang, J. Z. Liang, and J. Z. Wang, "Effect of polyethylene glycol on the crystallization and impact properties of polylactide-based blends." *Polym. Adv. Technol.*, **26**, 465 (2015).
34. B. Samiul, K. Ahmed, A. Saito, A. Khosla, M. Kawakami, and H. Furukawa, "Development of multi-material 3D printer." *ECS Trans.*, **88**, 449 (2018).